

Elastic scattering of one-proton halo nucleus ^{17}F on different mass targets using semi microscopic potentials

Awad A. Ibraheem^{a,b}, Arwa S. Al-Hajjaji^c and M. El-Azab Farid^d

^a*Physics Department, King Khalid University, Abha, Saudi Arabia.*

^b*Physics Department, Al-Azhar University, Assiut 71524, Egypt.*

^c*Physics Department, Taiz University, Taiz, Yemen.*

^d*Physics Department, Assiut University, Assiut 71516, Egypt.*

Received 12 September 2018; accepted 9 November 2018

The elastic scattering of ^{17}F from different mass targets (^{12}C , ^{14}N , ^{58}Ni and ^{208}Pb) at different energies has been studied. We used the double folding optical model potential based on the density-dependent DDM3Y effective nucleon-nucleon interaction without need to renormalize the generated potentials. Two versions of the density distribution of the one-proton halo ^{17}F nucleus have been taken into account in order to derive the double folding potentials. The measured angular distributions of elastic scattering differential cross section and corresponding reaction cross sections have been successfully reproduced at different energies using the derived potentials. The energy and the target mass number dependences of imaginary volume integrals as well as the total reaction cross sections have been also studied.

Keywords: Optical model; elastic scattering; halo nuclei; folding model.

PACS: 25.70.Bc; 24.10.Ht; 27.20.+n.; 21.60.Gx

1. Introduction

The nuclei far from β stability line have attracted an immense interest since the first observation of the neutron halo in ^{11}Li [1]. Further experiments have confirmed the presence of neutron halo in ^{11}Li and other neutron-rich nuclei [2]. Through the last two decades, experimental data for the proton halo in proton-rich nuclei like ^8B , ^{17}Ne , and $^{26,27,28}\text{P}$ have been reported in literature [3-11]. However, the amount of experimental data on the proton halo is relatively small compared to those on the neutron halo. The short-lived radioactive nucleus ^{17}F is one of the candidates for a proton-halo nucleus due to its small (600 keV) proton separation energy. But, it cannot be studied with usual spectroscopic techniques due to its short lifetime. Hence, one must resort to indirect methods to deduce information about its structure. Reactions are the most used tools to study halo nuclei. Elastic scattering [12,13] and breakup [14,15] provide interesting information about the structure of the projectile. Therefore, many experiments with ^{17}F as projectile have been performed in recent years [16-27]. It is important to mention that, the $^{16}\text{O}(\text{p}, \gamma)^{17}\text{F}$ capture cross section measured in through the energy range $E_{c.m.} = 200 - 3750$ keV covers five orders of magnitude of cross sections. Some data give striking different energy dependences of the branching ratio between the transition to the $5/2^+$ ground state and to the $1/2^+$ first excited state of ^{17}F which is bound by only 105 keV. On the other hand, the $^{16}\text{O}(\text{He}, \text{d})^{17}\text{F}$ reaction was used to determine asymptotic normalization coefficients for transitions to the ground and first excited states of ^{17}F . Full coupled channels calculations were performed to study the $^{16}\text{O}(\text{d}, \text{p})^{17}\text{F}$ and the $^{16}\text{O}(\text{d}, \text{n})^{17}\text{F}$ transfer reactions at sub-Coulomb energies ($E_d = 2 - 3$ MeV) [27-29].

On the other side, through the past three decades, nucleus-nucleus optical model (OM) potentials have been studied extensively through elastic scattering measurements. The observed data were interpreted in the framework of both phenomenological and microscopic double folding (DF) potential models with the adjustment with none and with only a few parameters [20-37]. In the present work, we have applied the DF model to analyze the elastic scattering of ^{17}F nucleus on light-mass targets (^{12}C , ^{14}N), medium-mass target (^{58}Ni), and on ^{208}Pb which is an example of a heavy target. The paper is organized as follows: In Sec. 2, we give a brief account of the adopted formalism. The procedure is discussed in Sec. 3. Results and discussion, and their comparison with the available experimental data are listed in Sec. 4, while concluding remarks are finally presented in Sec. 5.

2. Theoretical Formalism

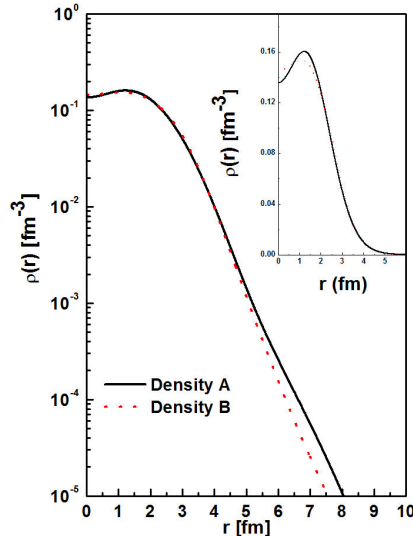
The real nucleus-nucleus optical potential in the DF model is given by the expression [31]

$$V_{DF}(R) = \iint \rho_p(r_1) \rho_T(r_2) v_{nn}^{DDM3Y}(s, \rho, E) dr_1 dr_2, \quad (1)$$

where $\rho_p(r_1)$ and $\rho_T(r_2)$ are the nuclear matter density distributions for projectile and target nuclei, respectively, and $v_{nn}(s)$ is the effective nucleon-nucleon (NN)

interaction with $s = |\vec{R} - \vec{r}_1 + \vec{r}_2|$ the distance between the two nucleons. In the present calculation, we use the most popular density-dependent DDM3Y, effective NN interaction of Bertsch *et al.* [38] which has the following form [31]

$$v_{nn}^{DDM3Y}(s, \rho, E) = f(\rho, E) v_{nn}^{M3Y}(E, s) \quad (2)$$

FIGURE 1. Comparison between the two densities A and B of ^{17}F .

The functional form of this density and energy dependent factor, $f(\rho, E)$ is chosen as

$$f(\rho, E) = C(E)(1 + \alpha(E)) \exp(-\beta(E)\rho). \quad (3)$$

The M3Y interaction is taken in the form

$$v_{nn}^{DDM3Y}(E, s) = 7999 \frac{\exp(-4s)}{4s} - 2134 \times \frac{\exp(-2.5s)}{2.5s} + 276(1 - 0.005E)\delta(s) \quad (4)$$

where the third energy-dependent term is a zero range pseudo-potential to account for the single nucleon exchange effect and E is the laboratory energy per nucleon. For the projectile ^{17}F nucleus, two versions of nuclear matter density are considered. First, it is presumed that the ^{17}F nucleus consists of an ^{16}O core and a halo of one proton. The core density distribution is assumed to be of a harmonic oscillator (HO) form as [39]

$$\rho_c(r) = \rho_{160}(r) = 0.1317(1 + 0.6457r^2) \times \exp(-0.3228r^2) \text{ fm}^{-3} \quad (5)$$

where the halo density distribution is described by the Gaussian function as [35]:

$$\rho_h(r) = \rho_{1P}(r) = \left(\frac{3}{2\pi R_h^2} \right)^{3/2} \left(\frac{3r^2}{2R_h^2} \right) \text{ fm}^{-3} \quad (6)$$

TABLE I. The best fit imaginary WS potential parameters obtained from the analysis of nine sets of ^{17}F elastic scattering cross sections. The corresponding real and imaginary volume integrals (J_V and J_W , respectively), the total reaction cross section (σ_R), and χ^2 are also tabulated.

E_{lab} MeV	Density	W_0 (MeV)	r_W (fm)	a_W (fm)	J_V (Mev fm 3)	J_W (MeV fm 3)	σ_R (mb)	χ^2
$^{17}\text{F} + ^{12}\text{C}$								
170	A	24.1	1.17	0.68	343.65	103.86	1665	8.1
	B	51.14	1.15	0.56	343.65	201.57	1645	13.1
$^{17}\text{F} + ^{14}\text{N}$								
170	A	12.0	1.37	0.54	336.45	71.28	1736	9.3
	B	13.80	1.32	0.50	336.45	72.99	150	11.6
$^{17}\text{F} + ^{58}\text{Ni}$								
51.94	A	42.4	1.39	0.26	296.40	130.41	396.9	0.08
	B	42.22	1.38	0.25	296.0	127.01	421.5	0.43
170	A	45.3	1.24	0.68	312.69	105.12	2613	0.35
	B	51.14	1.31	0.49	312.69	134.93	2466	0.97
$^{17}\text{F} + ^{208}\text{Pb}$								
86	A	8.71	1.38	0.25	278.95	16.71	3.14	0.08
	B	10.8	1.33	0.33	278.95	18.62	4.56	0.09
90.4	A	8.71	1.38	0.25	278.71	16.71	34.5	0.64
	B	10.8	1.33	0.33	278.71	18.62	36.61	0.60
98	A	11.89	1.38	0.25	278.30	22.80	320.4	0.89
	B	12.46	1.33	0.35	278.30	21.54	328.0	0.86
120	A	29.00	1.30	0.53	264.78	47.34	1418	0.41
	B	38.07	1.30	0.48	264.78	61.89	1387	0.33
170	A	30.70	1.25	0.61	286.39	44.89	2420	0.12
	B	36.65	1.28	0.46	286.39	57.09	2312	0.14

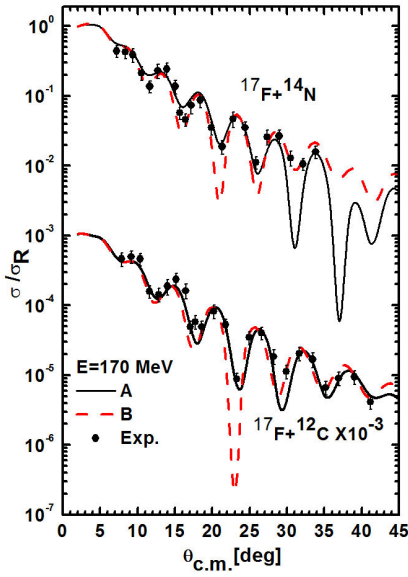


FIGURE 2. Angular distributions of the elastic scattering differential cross section relative to the Rutherford one for the $^{17}\text{F} + ^{12}\text{C}$ and $^{17}\text{F} + ^{14}\text{N}$ reactions using the DDM3Y potentials at $E_{\text{lab}} = 170$ MeV. Experimental data are taken from Ref. [23].

where $R_h = 3.78$ fm. Therefore, the total matter distribution $\rho_{^{17}\text{F}}$ (normalized to one nucleon) and the matter radius R_m are given as [40]:

$$\rho_{^{17}\text{F}}(r) = [16\rho_c(r) + (A - 16)\rho_h(r)]/A \quad (7)$$

$$R_m = \left(\frac{16R_c^2 + (A - 16)R_h^2}{A} \right)^{1/2} \quad (8)$$

This density produces a rms radius, $\langle r_{\text{rms}}^2 \rangle^{1/2}$ of ^{17}F equals to 2.77 fm. We denote this density as version A. In the second approach the density of ^{17}F nucleus is taken from Ref. [40]. This density produces a rms radius $\langle r_{\text{rms}}^2 \rangle^{1/2}$ of ^{17}F which equals to 2.74 fm. We denote this density as a version B. Figure 1 shows a comparison between the two considered A and B densities. It is evident that both densities have identical radial distributions over the range $r = 0 - 5$ fm as shown in the inset layer in Fig. 1. In the surface region ($r > 5$ fm) the density A has more extended tail than that of the B form. This indicates that the halo structure is more pronounced for the density A than the density B.

For the target nuclei ^{12}C and ^{14}N the nuclear matter density has been taken in the harmonic oscillator (HO) form [33,42]:

$$\rho_{^{12}\text{C}}(r) = 0.1644(1 + 0.4988r^2) \exp(-0.3741r^2) \quad (9)$$

$$\rho_{^{14}\text{N}}(r) = 0.15501(1 + 0.601358r^2) \exp(-0.3601r^2). \quad (10)$$

These densities yield rms radii $\langle r_{\text{rms}}^2 \rangle^{1/2}$ equal to 2.407 and 2.48 fm for ^{12}C and ^{14}N respectively. For the target nuclei ^{58}Ni and ^{208}Pb the nuclear matter density has been taken in the two parameter fermi form [34-37]

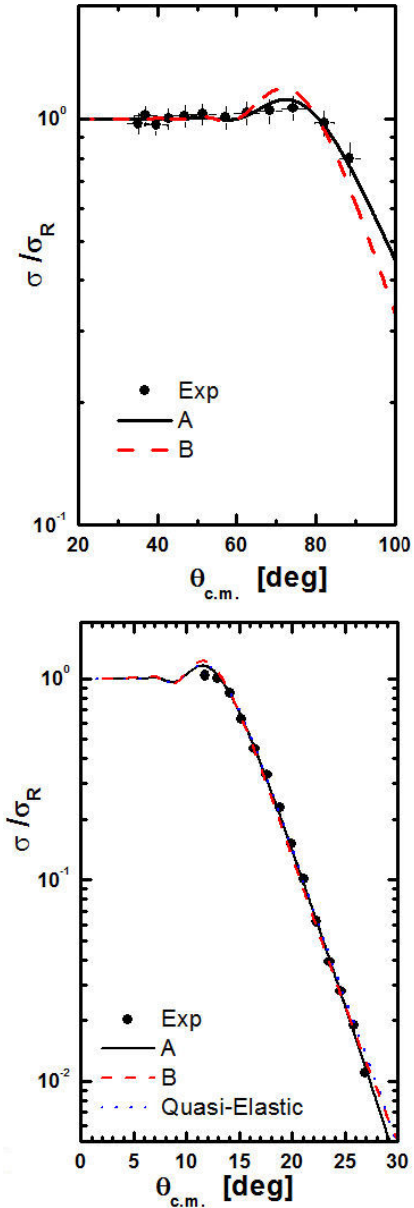


FIGURE 3. Same as Fig. 2, but for $^{17}\text{F} + ^{58}\text{Ni}$ reaction at $E = 51.94$ and 170 MeV. Experimental data are taken from Ref. [24,26].

$$\rho_{^{58}\text{Ni}}(r) = \frac{0.172}{1 + \exp(\frac{r-4.094}{0.54})} \quad (11)$$

$$\rho_{^{208}\text{Pb}}(r) = \frac{0.15}{1 + \exp(\frac{r-6.80}{0.515})}. \quad (12)$$

These densities yield rms radii $\langle r_{\text{rms}}^2 \rangle^{1/2}$ equals to 3.745 and 5.482 fm, respectively.

3. Procedure

The DF optical potentials generated from Eq. (1) using the density-dependent DDM3Y effective NN interaction are used

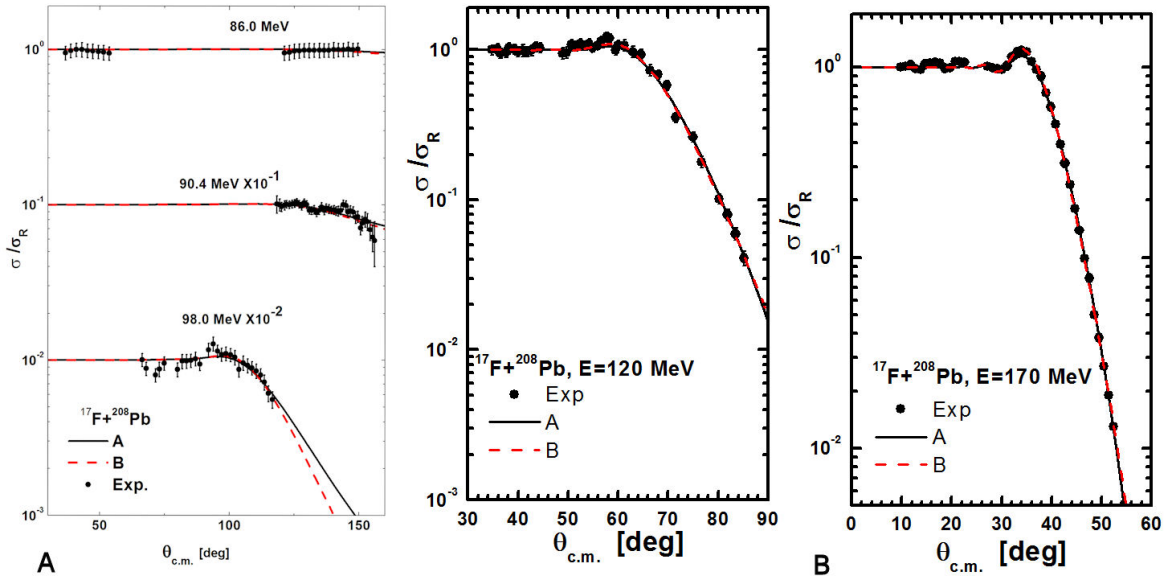


FIGURE 4. A: Same as Fig. 2, but for $^{17}\text{F} + ^{208}\text{Pb}$ reaction at $E = 86.0, 90.4$ and 98.0 MeV. Experimental data are taken from Refs. [25,22, 21], respectively. B: Same as Fig. 2, but for $^{17}\text{F} + ^{208}\text{Pb}$ reaction at $E = 120$ and 170 MeV. Experimental data are taken from Ref. [21,24].

to analyze the ^{17}F elastic scattering data. The DF potentials have been developed by considering the procedures given below:

- (1) The spin-orbit potential has been neglected. It is well known fact that the elastic scattering cross section data in this energy range are not sensitive to this potential [41].
- (2) The computer code DOLFIN [45] based on the Fourier-transform technique [32] has been used for this purpose.
- (3) The obtained potentials is fed into the code HIOPTM-94 [46] to represent the real part of the optical potential, while the imaginary part of the optical potential is taken in the phenomenological volume Woods-Saxon (WS) shape as

$$W(R) = \frac{-W_0}{1 + \exp\left(\frac{R - R_w}{a_w}\right)} \text{ MeV},$$

$$R_w = r_w \left(A_p^{1/3} + A_T^{1/3} \right) \quad (13)$$

where W_0 , r_w and a_w are the depth, radius and diffuse-ness parameters, respectively. Renormalization factors are not considered for the derived real microscopic DF potentials in order to optimize the fits with data.

- (4) The resulted potentials are used to analyze nine sets of data of the elastic scattering differential cross section for the following reactions:
 1. $^{17}\text{F} + ^{12}\text{C}$ at energy $E_{\text{lab}} = 170$ MeV.
 2. $^{17}\text{F} + ^{14}\text{N}$ at energy $E_{\text{lab}} = 170$ MeV.

3. $^{17}\text{F} + ^{58}\text{Ni}$ at energies $E_{\text{lab}} = 51.94$, and 170 MeV.
4. $^{17}\text{F} + ^{208}\text{Pb}$ at energies $E_{\text{lab}} = 86, 90.4, 98, 120$, and 170 MeV.
5. The routine searches have been carried out by considering an average value of 10% for all experimental errors of the considered data to minimize the value, which is represented as [31]

$$\chi^2 = \frac{1}{2} \sum_{i=1}^N \left[\frac{\sigma_{\text{cal}}(\theta_i) - \sigma_{\text{exp}}(\theta_i)}{\Delta\sigma_{\text{exp}}(\theta_i)} \right]^2 \quad (14)$$

where $\sigma_{\text{cal}}(\theta_i)$ and $\sigma_{\text{exp}}(\theta_i)$ are the theoretical and experimental cross sections, respectively, at angle, θ_i , $\Delta\sigma_{\text{exp}}(\theta_i)$ is the experimental error, and N is the number of data points.

4. Results and Discussion

The derived DF potentials based on the density-dependent DDM3Y effective NN interaction is used to analyze the elastic scattering of ^{17}F nucleus on ^{12}C , ^{14}N , ^{58}Ni and ^{208}Pb targets without renormalization factor. The obtained elastic scattering differential cross sections for the considered reactions are listed in Table I. These results are plotted as shown in Figs. 2-4 compared with the corresponding experimental data. The solid and dashed curves represent the results using, respectively, the density distribution A and B of the one-proton halo ^{17}F nucleus. We used the calculated DF potential to analyze the elastic scattering experimental data of $^{17}\text{F} + ^{12}\text{C}$, ^{14}N reactions as examples of the light-mass targets for only one energy value of $E_{\text{lab}} = 170$ MeV. As shown

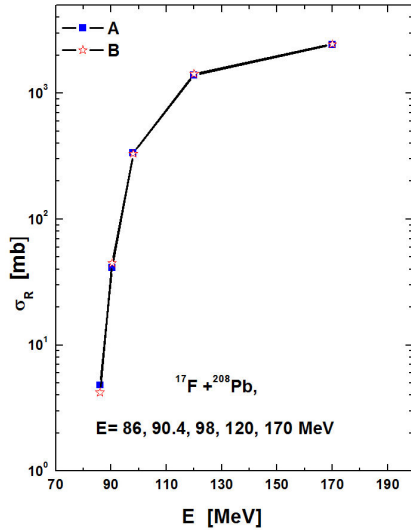


FIGURE 5. The energy dependence of the reaction cross-section for $^{17}\text{F} + ^{208}\text{Pb}$ system.

in Fig. 2, our results using the WS and microscopic DF potentials based on the JLM effective NN interaction are in good agreement with the corresponding measured data by Blackmon *et al.* [23]. For the medium mass targets, the elastic scattering data of $^{17}\text{F} + ^{58}\text{Ni}$ at $E = 51.94$ and 170 MeV measured by Liang *et al.* [24] Mazzocco *et al.* [26], as shown in Fig. 3, are well reproduced by our calculated potentials. It should be mentioned that, the effect of the quasi-elastic scattering is very weak. However, in our calculations, the coupled channel calculations using the cluster form factor for $^{17}\text{F} \rightarrow ^{16}\text{O}$ (core)+p (valence) as coupling between $(5/2)^+$ ground and $(1/2)^+$ states of ^{17}F are carried out as shown with dot lines in Fig. 3. For this purpose, we used only pure elastic scattering.

The obtained parameters of the imaginary phenomenological WS potentials, the corresponding real and imaginary volume integrals per interacting nucleon pair (J_V and J_W) in MeV fm³ and the total reaction cross sections σ_R in mb are listed in Table I. We have also studied the elastic scattering of ^{17}F from the heavy target ^{208}Pb . The elastic scattering angular distributions of $^{17}\text{F} + ^{208}\text{Pb}$ were measured at 98 MeV and 120 MeV [21], 90.4 MeV [22], 170 MeV [24], and 86 MeV [25]. We used the calculated DF potentials for this system to describe the experimental data at these energies. The results of our calculations for the $^{17}\text{F} + ^{208}\text{Pb}$ system are presented in Fig. 4 compared with the experimental data. At energies of 86 , 90.4 and 98 MeV, the calculated angular distributions of the differential cross section produced reasonable agreements with experimental data for the three considered energies as shown by the solid and dashed lines in Fig. 4, except the few forward angles data ($\theta_{c.m.} > 90^\circ$) at 98 MeV case and the few backward angles data ($\theta_{c.m.} > 150^\circ$) at 86 and 90.4 MeV. For energies 120 and 170 MeV, successful reproduction of data is obtained. Also, it is evident from these figures that the present predictions for the 120 and 170 MeV data are more successful than those predicted for the 86 , 90.4

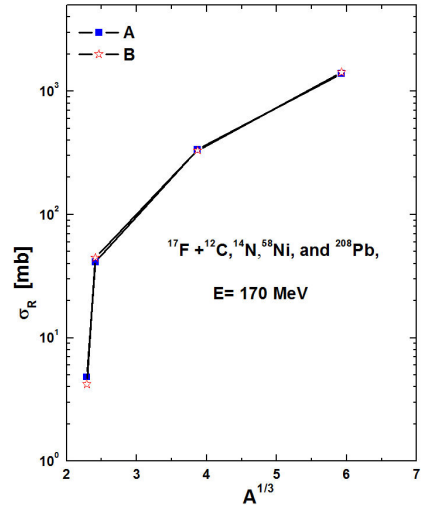


FIGURE 6. The target mass-number dependence of the reaction cross-section for $^{17}\text{F} + ^{12}\text{C}$, $^{17}\text{F} + ^{14}\text{N}$, $^{17}\text{F} + ^{58}\text{Ni}$ and $^{17}\text{F} + ^{208}\text{Pb}$ systems at $E_{\text{lab}} = 170$ MeV.

and 98 MeV. It is noticed from these figures and the values of χ^2 shown in Table I that fits with data obtained using the version A of the density distribution of the ^{17}F nucleus is better than those resulted using version B. An additional important piece of information that can be deduced from the elastic scattering analysis, is the total reaction cross section as well as the determination of the Coulomb barrier [46,47]. The Coulomb barrier strength V_B and radius R_B can be determined from the following equations:

$$V_B = \frac{Z_p Z_T e^2}{R_B} - \frac{15}{x+1}, \quad (15)$$

$$x = 27.1 \frac{(A_p^{1/3} + A_T^{1/3})}{Z_p Z_T},$$

$$R_B = 1.3(A_p^{1/3} + A_T^{1/3}) + 0.65 \ln(x), \quad (16)$$

which yield $V_B = 8.6$, 10 , 36 and 78 MeV respectively for ^{12}C , ^{14}N , ^{58}Ni and ^{208}Pb target nuclei. This information is useful to investigate the role of breakup (or other reaction mechanisms) for weakly bound exotic nuclei.

The obtained reaction cross section values for all considered reactions are given in Table I. The extracted values are quite consistent with those reported in recent studies [21-26]. The obtained total reaction cross sections, σ_R , for $^{17}\text{F} + ^{208}\text{Pb}$ system are plotted versus the energy E , as shown in Figs. 5, 6. We observe that for all considered energies, σ_R increases with increasing the energy E . The target mass-number dependence of the reaction cross-section for all considered systems at $E_{\text{lab}} = 170$ MeV is shown also in this figure. The reaction cross-section increases with increasing the cubic root of the target mass number $A^{1/3}$. To investigate the energy dependence of the imaginary volume integral, we plotted the calculated imaginary volume integral J_W , listed in Table I, against the energy E for $^{17}\text{F} + ^{208}\text{Pb}$ reaction.

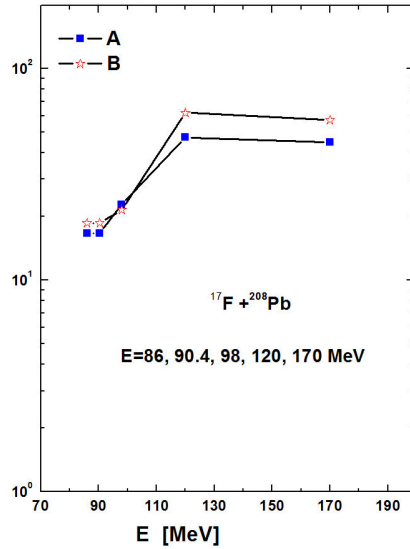


FIGURE 7. The energy dependence of the imaginary volume integral for $^{17}\text{F} + ^{208}\text{Pb}$ reaction.

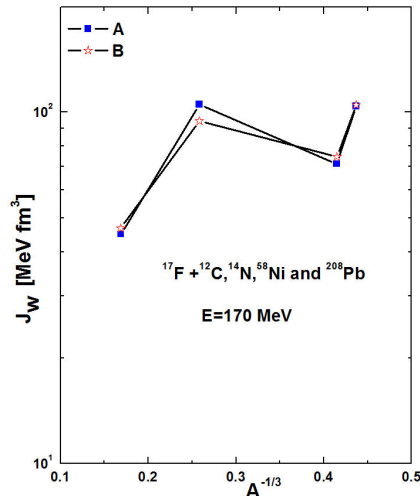


FIGURE 8. The target mass-number dependence of the imaginary volume integral for $^{17}\text{F} + ^{12}\text{C}$, $^{17}\text{F} + ^{14}\text{N}$, $^{17}\text{F} + ^{58}\text{Ni}$ and $^{17}\text{F} + ^{208}\text{Pb}$ systems at $E_{\text{lab}} = 170$ MeV.

The imaginary J_W values does not show a clear behavior with energy for the DF potential. Also, we plotted the calculated imaginary volume integral J_W , listed in Table I, against the cubic root of the target mass number $A^{1/3}$ for all considered systems at 170 MeV as shown in Figs. 7, 8.

5. Conclusions

In the present work, we have analyzed the elastic scattering data for ^{17}F nucleus on light-mass targets (^{12}C , ^{14}N), medium-mass target (^{58}Ni), and heavy-mass target (^{208}Pb) at different energies in the framework of the OM. The DF model is employed to generate the real part of the optical potentials, by folding the density-dependent DDM3Y effective NN interaction over two versions of the density distribution of the one-proton halo ^{17}F nucleus besides the density of targets, while the imaginary part is treated phenomenologically through the WS form. Successful predictions of different sets of data at above the Coulomb barrier energies are obtained all over the measured angular ranges without needing to renormalize the generated potentials. Furthermore, the total absorption (reaction) cross sections for the four reactions are investigated. It is found that, the extracted values from the present elastic scattering calculations agree well with the measured data. The energy- and target mass number-dependences have been checked for the resulted reaction cross sections from the derived DF potentials at 170 MeV for the $^{17}\text{F} + ^{208}\text{Pb}$ reaction.

Acknowledgments

The authors extend their appreciation to the Deanship of Scientific Research at King Khalid University for funding this work through research groups program under grant number R.G.P.1/6/40.

1. I. Tanihata *et al.*, *Phys. Rev. Lett.* **55** (1985) 2676.
2. A. S. Jensen and M. V. Zhukov, *Nucl. Phys. A* **693** (2001) 411.
3. T. Minamisono *et al.*, *Phys. Rev. Lett.* **69** (1992) 2058.
4. M. Fukuda *et al.*, *Nucl. Phys. A* **656** (1999) 209.
5. D. Cortina-Gil *et al.*, *Nucl. Phys. A* **720** (2003) 3.
6. E. F. Aguilera *et al.*, *Phys. Rev. C* **79** (2009) 021601(R).
7. A. Barioni *et al.*, *Phys. Rev. C* **84** (2011) 014603.
8. V. Morcelle *et al.*, *Phys. Rev. C* **95** (2017) 014615.
9. R. Kanungo *et al.*, *Phys. Lett. B* **571** (2003) 21.
10. K. Tanaka *et al.*, *Nucl. Phys. A* **746** (2004) 532c.
11. A. Navin *et al.*, *Phys. Rev. Lett.* **81** (1998) 5089.
12. T. Matsumoto *et al.*, *Phys. Rev. C* **73** (2006) 051602(R).
13. A. Di Pietro *et al.*, *Phys. Rev. Lett.* **105** (2010) 022701.
14. N. Fukuda *et al.*, *Phys. Rev. C* **70** (2004) 054606.
15. D. Baye, P. Capel and G. Goldstein, *Phys. Rev. Lett.* **95** (2005) 082502.
16. H. Kitagawa, N. Tajima and H. Sagawa, *Z. Phys. A* **358** (1997) 381.
17. K. E. Rehm *et al.*, *Phys. Rev. Lett.* **81** (1998) 3341.
18. J. F. Liang *et al.*, *Phys. Lett. B* **491** (2000) 23.
19. A. Ozawa, T. Suzuki and I. Tanihata, *Nucl. Phys. A* **693** (2001) 32.

20. J. F. Liang *et al.*, *Phys. Rev. C* **65** (2002) 051603.
21. J. F. Liang *et al.*, *Phys. Rev. C* **67** (2003) 044603.
22. M. Romoli *et al.*, *Phys. Rev. C* **69** (2004) 064614.
23. J. C. Blackmon *et al.*, *Phys. Rev. C* **72** (2005) 034606.
24. J. F. Liang *et al.*, *Phys. Lett. B* **681** (2009) 22.
25. C. Signorini *et al.*, *Eur. Phys. J. A* **44** (2010) 63.
26. M. Mazzocco *et al.*, *Phys. Rev. C* **82** (2010) 054604.
27. N. Patronis *et al.*, *Phys. Rev. C* **85** (2012) 024609.
28. R. Morlock *et al.*, *Phys. Rev. Lett.* **79** (1997) 3837.
29. C. A. Gagliardi *et al.*, *Phys. Rev. C* **59** (1999) 1149.
30. M. Assunção *et al.*, *Phys. Rev. C* **70** (2004) 054601.
31. G. R. Satchler and W. G. Love, *Phys. Rep.* **55** (1979) 183.
32. M. E. Brandan and G. R. Satchler, *Phys. Rep.* **285** (1997) 143.
33. M. El-Azab Farid and M. A. Hassanain, *Nucl. Phys. A* **678** (2000) 39.
34. M. El-Azab Farid and M. A. Hassanain, *Nucl. Phys. A* **697** (2002) 183.
35. M. El-Azab Farid and M. A. Hassanain, *Eur. Phys. J. A* **19** (2004) 231.
36. L. C. Chamon *et al.*, *Phys. Rev. Lett.* **79** (1997) 5218.
37. L. C. Chamon, D. Pereira, M. S. Hussein, *Phys. Rev. C* **58** (1998) 576.
38. G. Bertsch *et al.*, *Nucl. Phys. A* **284** (1977) 399.
39. G. D. Alkhazov *et al.*, *Nucl. Phys. A* **712** (2002) 269.
40. Reference Input Parameter Library (RIPL-2), <http://www-nds.iaea.org/RIPL-2>
41. J. P. Vary and C. B. Dover, *Phys. Rev. Lett.* **31** (1973) 1510.
42. A. Nadasen *et al.*, *Phys. Rev. C* **47** (1993) 674.
43. L.D. Rickertsen, (unpublished).
44. N.M. Clarke, (1994) (unpublished).
45. K. C. C. Pires , S. Appannababu and R. Lichtenhäler, *Few-Body Syst* **57** (2016) 315.
46. A. S. Freitas *et al.*, *Braz J Phys* **46** (2015) 120